Heterogeneous Rate Coupling for Graphite Oxidation

J. R. Baron* and H. Bernstein†
ManLabs Inc., Cambridge, Mass.

Surface oxidation of a refractory material upon exposure to a high-temperature flowfield is assessed on the basis of a surface coupled model. The appearance of limiting phenomenological behavior is not presumed. The formulation allows for both gaseous and solid oxide formations as a result of Arrhenius relations for oxidation kinetics at the gas-solid interface. Numerical results are presented for the case of a laminar boundary layer adjacent to a graphite stagnation point assuming gas phase equilibrium and multicomponent variable transport properties. Multiple mass transfer plateaus are found to be present, each plateau corresponding to a diffusion limit behavior over a surface temperature interval in which a specific gaseous oxide proves to be dominant. Reaction constant magnitudes effectively dictate the transition behavior between plateaus, the departure from the low-temperature reaction controlled region, and the widths of the surface temperature intervals over which individual plateaus are distinct. For graphite recession, the sensitivity of such effects is appreciable relative to uncertainties in rate data.

Nomenclature

a	=	solid oxide parameter
a_{ij}	=	relative number of ith kind in jth component
$c_i, \bar{c}_i$	=	mass fraction, ρ_i/ρ; same from all sources, $\Sigma(m_i/m_j)a_{ij}c_j$
$\bar{c}_p$	=	normalized specific heat, c_p/c_{p_w}
$\mathfrak{D}_{ij}$	=	binary mass diffusion coefficient
ΔF_j^0	=	molar free energy of formation
g_i	=	total convective and diffusive mass flux of ith kind
$\bar{h}$	=	normalized enthalpy, $h/(c_pT)_e$
Δh_y^0	=	molar enthalpy of formation
J_{m_i}, J_i	=	mass diffusion flux; same for similarity form
k	=	number of elements
k_i	=	rate constant
$L_{ij}, \mathfrak{L}_{ij}$	=	Lewis number, $\rho c_p D_{ij}/\kappa$; binary Lewis number, $\rho c_p \mathfrak{D}_{ij}/\kappa$
R_B	=	stagnation-point radius of curvature
X_i	=	mole fraction of ith kind
$\bar{\gamma}$	=	modified specific heat ratio, $m_e c_p/R$
ϵ	=	mean square error
λ	=	$(\rho\mu)/(\rho\mu)_w$
ν	=	number of components
θ, θ_A	=	normalized temperature, T/T_e; same for activation
Γ_i, Γ_q	=	mass flux parameter; same for energy
$(\ )_e, (\ )_w$	=	external edge of layer; reacting surface

I. Introduction

REFRACTORY oxidation is a complex surface problem which frequently involves a correspondingly complicated coupling with the fluid processes immediately adjacent to the gas-solid interface. Such coupling differs markedly for different test situations, as indicated by the response of refractory materials at elevated temperatures when imposed during arc plasma re-entry simulation as contrasted to a furnace environment.[1] This study specifically considers the coupling influence on the recession rate of a graphite surface under typical hypersonic flight conditions.[2] It is believed, however, that the findings have some bearing on general refractory response.

Mass transfer resulting from surface oxidation at very high speeds has received attention for several years in exact and approximate forms.[3–5] The crucial assumption for purposes of simplicity in exact solutions has been the sufficiency of an independent evaluation of injection effects on the gas phase behavior. The resulting constraint on the surface rate process has been referred to as a "diffusion limited" description on the basis of a balance between the rates of oxygen consumption and its supply to the surface by diffusion through the boundary layer. This is inferred for an intermediate surface temperature range; at lower and higher temperatures "reaction limited" and "vaporization limited" regimes are present in fact. The former implies oxidation proceeding with complete independence of the boundary-layer presence; the latter assumes equilibrium vaporization essentially superimposed upon the diffusion limit. Transitions between all such limiting situations are required and have been suggested on an empirical basis.

Such phenomenological models fundamentally examine events when either the diffusive or reaction speed dominates. The effect is to uncouple the gas-phase and surface chemistry behaviors. When applicable such concepts are clearly quite useful, especially in view of associated scaling rules, for test planning and evaluation as well as design. At a minimum some verification is required for the appropriateness of such models for typical surface materials operating in specific environments of interest. Experimental comparisons have made possible a degree of acceptability for either coupled or uncoupled models, primarily as a result of both scatter in the data and the nature of the difference for the results.

This is of particular importance in view of the frequent neglect of coupling influences when determining the fundamental rate constants. Such values often may be used, in fact, only under the very special circumstances for which they were obtained, both quantitatively and qualitatively. In this respect the present study may be of interest for other than hypersonic applications.

For both of these reasons the essential provision in this study is an allowance for the appearance of limiting rate situations without presuming their existence under any set of physical operating conditions: i.e., neither limiting behavior nor a fixed rate constant specification were assumed. Several numerical descriptions were employed instead as representative of the uncertainty in graphite surface kinetics, all of an Arrhenius form with allowance for gas surface equilibrium to be achieved. The adjacent laminar boundary layer was restricted to gas-phase chemical equilibrium with multicomponent and variable transport properties. Nu-

Presented as Paper 70823 at the AIAA 5th Thermophysics Conference, Los Angeles, Calif., June 29–July 1, 1970; submitted July 31, 1970; revision received December 3, 1970. Investigation sponsored by Air Force Materials Laboratory, Air Force Systems Command, Contract AF33(615)-3859.

* Consultant. Associate Fellow AIAA.
† Senior Staff.

merical results were obtained for a stagnation-point flow on the basis of similarity.

Exact solutions to problems of this kind prove difficult primarily due to the necessary inclusion of numerous gaseous components. In particular, complications arise due to: 1) mass action statements and constraints for allowed reactions; 2) algebraically extensive specifications for multicomponent transport properties; 3) the exponential nature of both rate and equilibrium relations, which lead to several orders of magnitude changes in prime variables (e.g., oxygen concentration) of direct importance to the surface reaction; and 4) the two-point boundary condition nature which requires considerable iterative skill to establish a consistent set of component concentrations.

In the following, a substantial reduction in numerical complexity was achieved by use of a flux integration procedure suggested by Nachtsheim.[6] This eliminates the need for explicit and repetitive evaluations of multicomponent transport properties involving cumbersome mass diffusion coefficient matrices. The required binary diffusion coefficients were based on very accurate empirical fits according to the simplified procedure of Bartlett, Kendall, and Rindal.[7]

Oxide production was limited to carbon monoxide and dioxide in the examples considered, although the formulation includes a possible solid oxide formation to indicate its role. The basic air model was chosen to be four component dissociated air primarily ($\nu = 6$), but with brief consideration given to nitric oxide to evaluate its importance ($\nu = 7$). Surface kinetics were purposely chosen to appreciably vary the rapidity with which oxygen consumption occurs at the boundary. Two such specifications were those suggested by Scala[3] as brackets for available graphite data and designated "fast" and "slow." A third and more recent suggestion[1] implies still "slower" kinetics after attempts to introduce diffusion coupling influences into actual evaluation of the fundamental rate constant. Essentially, this amounted to a simplified accounting for the variation of the partial pressure of oxygen during transition from reaction to diffusion control for the process. The three descriptions are both representative and afford comparison with previous predictions of graphite recession behavior.

II. Formulation

The problem may be described by a set of conservation statements for the laminar boundary layer adjacent to the reacting surface and in which all transport effects are confined. Conditions imposed at the surface and the external edge of the layer constrain the rates at which energy, oxygen, and surface components are supplied to or from the boundary. At a stagnation point the convenient similarity description is given by‡

$$[(\lambda/Pr)\sum_j (m_i m_j/m^2)L_{ij}X_j']' - m_i f(X_i/m)' = \dot{w}_i/2\rho du_e/dx \quad (i = 1, \ldots, \nu - 1) \quad (1a)$$

$$(\lambda f'')' + ff'' + \tfrac{1}{2}(\rho_e/\rho - f'^2) = 0 \quad (1b)$$

$$\left(\frac{\lambda \bar{c}_p}{Pr}\theta'\right)' + \left(\bar{c}_p f - \frac{\lambda}{Pr}\sum_i \bar{c}_{p_i}\sum_j \frac{m_i m_j}{m^2}L_{ij}X_j'\right)\theta' = \frac{\bar{c}_{p_e}\sum_i h_i \dot{w}_i}{2\rho(du_e/dx)(c_p T)_e} \quad (1c)$$

for the ith component mass, momentum and energy conservation of a ν component mixture. The mass rate of production per unit volume $\dot{w}_j$ vanishes for inert components or alternatively is constrained by the interdependent mole fractions X_i in equilibrium. It is therefore advantageous to restructure the $(\nu - 1)$ Eqs. (1a) into a lesser number of "element" relations plus auxiliary algebraic equilibrium statements. For k elements ($1 \leq k \leq \nu$), their conservation implies

$$\sum_{j=1}^{\nu} a_{ij}\left(\frac{m_i}{m_j}\right)\dot{w}_j = 0 \qquad (i = 1, \ldots, k) \quad (2)$$

where a_{ij} refers to the relative number of "atoms" of the ith "element" in the jth component. The weighted sum of Eqs. (1a) then eliminates the source terms, and the remaining $(\nu - 1 - k)$ relations are the required mass action rules for the X_i at some p. Similarly, the source terms in the energy balance are reducible to a summation of products of enthalpy differences and k convective and diffusive equivalents of $\dot{w}_i$ upon substituting from Eqs. (1a).

The external flowfield specifies conditions at the layer's outer edge, i.e., velocity, altitude and geometry or equivalently i_e, p_e, $(p_x)_e$, and composition. In similarity form $f_e' = \theta_e = 1.0$, $\beta = 0.5$. For components originating from the surface the X_{i_e} vanish, and for air components the mole fractions follow from the overall edge proportion and equilibrium constants

$$\left(\frac{X_O + 2X_{O_2}}{X_N + 2X_N}\right)_e \text{ and } (K_{p_i})_e = \left(\frac{pX_i^2}{X_{i_2}}\right)_e \qquad (i = O,N) \quad (3)$$

and the constraint $\Sigma X_{i_e} = 1$.

At the surface the interphase mass transfer and gas-phase equilibrium introduce the problem's essential coupling between $(\rho v)_w$, T_w, and all X_{iw}. Allowing for possible solid oxide deposition but without vaporization, it is convenient to consider the illustrative surface reaction

$$A_n B_m(s) + z_0\bar{O} \rightleftarrows z_1 AO_y(s) + z_2 B_q O_r + z_3 B_s O_t \quad (4)$$

for the initial solid phase $A_n B_m (= S$, say) with interdependent stoichiometric coefficients z_i and all participating oxygen designated by $\bar{O}$. The reaction (4) proceeds at a rate

$$\dot{m}_S = \left[\sum_{i=O,O_2} k_i(p_i^{n_i} - p_{i_{eq}}^{n_i})\exp\left(-\frac{\theta_{A_i}}{\theta}\right)\right]_w \quad (5)$$

in terms of rate constants (k_i), activation temperatures (θ_{A_i}), reaction orders (n_i), and the surface interphase equilibrium level ($p_{i_{eq}}$).

Both molecular and convective contributions affect the surface mass flux of the individual components, i.e.,

$$g_{i_w} = (J_{m_i} + \rho_i v)_w \quad (6)$$

or in conformity with Eqs. (4) and (5)

$$g_{i_w} = \begin{cases} (m_i/m_S)z_i\dot{m}_S & (i = B_qO_r, B_sO_t) \\ -y(m_O/m_S)z_1\dot{m}_S & (i = \bar{O}) \\ 0 & (i = \bar{N}) \end{cases} \quad (7)$$

Thus, nitrogen is not directly involved in the surface reaction and solid oxides lead to a negative contribution to the oxygen flux. Over-all,

$$(\rho v)_w = \sum_1^{\nu} g_{i_w} = \left(1 - \frac{m_{AO_y}}{m_S}z_1\right)\dot{m}_S = \left[\sum_{i\neq N,N_2}^{\nu}\left(\frac{J_{m_i}}{c_N + c_{N_2}}\right)\right]_w \quad (8)$$

and illustrates both the coupling with the diffusive processes (J_{m_i} term) and the possibility of oxidation with a reduced or vanishing injection level (z_1 term).

The interface ($\eta = 0$) conditions summarized in similarity form are

$$f_w' = 0,\ \theta = \theta_w,\ -f_w = [1 - (m_{AO_y}/m_S)z_1]\dot{m}_S^*$$
$$(J_N + J_{N_2})_w = [(c_N + c_{N_2})fPr]_w$$
$$(X_{CO}f)_w = \frac{m}{m_{CO}}\left(\frac{J_{CO}}{Pr} - g_{CO}^*\right),\ (K_{p_i})_w = (X_i^2/X_{i_2})_w p$$
$$(i = O,N),\ (K_{pCO_2})_w = (X_{CO_2}/X_O X_{CO} p)_w \quad (9)$$

‡ Some details are included in the Appendix.

These include $(\nu - k)$ equilibrium relations and $(k - 1)$ equivalent element constraints. Starred quantities are normalized reaction rates and fluxes according to, e.g.,

$$\dot{m}_S^* = [\lambda p/2\mu R_B(du/dx)]_e^{1/2}(R_B/p\rho_e)^{1/2}\dot{m}_S \qquad (10)$$

in which Newtonian theory for a stagnation point suggests

$$R_B du_e/dx = [2(p_e - p)_\infty/\rho_e]^{1/2} \qquad (11)$$

Since the fundamental coupling process in Eq. (5) neither involves a geometric scale nor necessarily behaves as $p^{1/2}$, some departures from a diffusion controlled description, i.e., $\dot{m}_S(R_B/p)^{1/2} \sim$ const, are to be expected. This is most evident for the low surface temperature (reaction limit) case.

The heat flux from the surface is

$$q_w = -\kappa\frac{\partial T}{\partial y} + \sum_i h_i J_{mi} + (\rho v)_w[h_w - ah_S(s)] +$$

$$(a - 1)h_S(s) = \left(\frac{2\rho\mu du/dx}{\lambda}\right)_e^{1/2}(c_pT)_e\left[-\frac{\theta'}{\bar{c}_{pe}Pr} + \sum_i \bar{h}_i\left(\frac{J_i}{Pr} - c_i f\right) + \dot{m}_S^* H\right] \qquad (12)$$

$$(N_2,N,O_2,O)$$

where "a" accounts for the possible solid oxide and H includes contributions due to heats of reactions (see Appendix).

Flux Integration

Most of the difficulty associated with obtaining numerical solutions of Eqs. (1) subject to (9) are traceable to the two-point boundary conditions and the cumbersome algebraic description of multicomponent mass diffusion coefficients and their spatial derivatives. The latter problem may be avoided by use of Nachtsheim's[6] suggestion to introduce the Stefan-Maxwell relations. The essential point is the use of transport fluxes as dependent variables with later evaluation of component behavior on the basis of the flux distributions. Introducing the flux parameters

$$\Gamma_i = \frac{\lambda}{Pr}J_i,\ \Gamma_q = -\frac{\lambda\bar{\gamma}}{Pr}\theta' + \sum_1^\nu\left(\frac{m_e}{m_i}\right)\bar{h}_i^0\Gamma_i \qquad (13)$$

Eqs. (1a) and (1c) become

$$\Gamma_i' = fc_i' + \frac{\dot{w}_i}{2\rho}\Big/\frac{du_e}{dx} \qquad (i = 1, \ldots, \nu - 1),$$

$$\Gamma_q' = f\left[\bar{\gamma}\theta' + \sum_{i=1}^{\nu}\left(\frac{m_e}{m_i}\right)\bar{h}_i^0 c_i'\right] \qquad (14)$$

and Eq. (1b) remains unchanged. Considering Γ_i and Γ_q as dependent variables implies recovery of the necessary concentrations from the Stefan-Maxwell relations

$$X_j' = \sum_{i=1}^{\nu}\frac{Pr}{\lambda\mathfrak{L}_{ji}}\frac{m}{m_e}\left(\frac{m_e}{m_i}X_j\Gamma_i - \frac{m_e}{m_j}X_i\Gamma_j\right) \qquad (15)$$

showing the need for only binary diffusion coefficients. Knowledge of a consistent (not necessarily appropriate!) set of equilibrium X_i at some point (e.g., the surface) allows propagation of the X_i distributions successively with the Γ_i.

Table 1 Graphite reaction rate parameters

Reaction	$k_{O_2} n_{O_2}$ (lb/ft² sec atm)	T_{O_2} (°R)	n_{O_2}
Fast[3]	6.73×10^8	39,900	1/2
Slow[3]	4.47×10^4	38,300	1/2
Slower[1]	0.532	10,000	1/3

Table 2 O-N-C system diffusion factors for Eq. (18) approximation

Component i	Diffusion factor, Fi	Component i	Diffusion factor, Fi
N_2	1.0323	NO	1.0037
O_2	1.0000	CO	1.0220
C	0.6643	CO_2	1.2700
N	0.7383	C_3	1.0927
O	0.7399	CN	1.0350

The essential simplification is the introduction of a relatively simple set of ν linear equations which replace a calculation involving inversion of $\nu \times \nu$ diffusion coefficient matrices for multicomponent properties.[9]

At the external edge the boundary conditions remain of the same form, as does f_w', θ_w, and f_w at the surface, Eqs. (9). However, the surface mass diffusion flux conditions for the elements are replaced by the equivalent

$$\bar{\Gamma}_{iw} = f_w(\bar{c}_{iw} - \bar{g}_{iw}/(\rho v)_w) \qquad (i = 1, \ldots, k) \qquad (16)$$

in which $\bar{(\ )}$ implies total i from all sources are included, and the second term in the parentheses clearly represents that fraction of the over-all surface flux in which the element participates. Upon summing the individual g_{iw} to obtain $\bar{g}_{iw}$ the fraction leads to molecular mass ratios; e.g., for the choice of "elements" as $i = N_2, O_2, CO$, the result is 0, $-m_O/m_C$, m_{CO}/m_C, respectively. The integration procedure involves $k + 1$ additional surface conditions as initial guesses, these being f_w'', Γ_{qw}, and X_{iw} (or c_{iw}) for $i = 1, \ldots, k - 1$.

III. Physical Conditions and Numerical Procedures

Numerical evaluations were completed for graphite oxidation at surface temperatures, stagnation pressures, and nose radii in the ranges $1500 \leq T_w$, °R ≤ 5500, $0.0585 \leq p$, atm ≤ 5.85, and $10^{-2} \leq R_B$, ft ≤ 1, all for an external edge temperature of 12,590°R ($h_e = 8304$ Btu/lb). Stagnation-point conditions of 5.85 atm and 12,590°R correspond to flight at 100,000 ft alt and 20,000 fps velocity, and were selected in part for purposes of comparison with earlier predictions.

Table 1 lists the three reaction descriptions that were considered. "Slow" and "fast" refer to limiting values suggested by Scala[3] after a literature review while "slower" refers to a more recent suggestion.[1]

Thermodynamic properties ($h_j^0, c_{pj}^0, \Delta h_j^0, \Delta F_j^0$) were introduced by means of quadratic (Gram Polynomial least squares) curve fitting to JANAF[8] tabulations for the range $500 \leq T$, °K ≤ 5500. A consistent and accurate representation then follows for the mixture properties. For example, with such quadratics for $h_j^0 (j \leq k)$ and $\Delta F_j^0 (j > k)$ it follows that

$$h_j^0 = \Delta F_j^0 - T\frac{d\Delta F_j^0}{dT} + \sum_{i=1}^{k} a_{ji}h_i^0 \ (j > k) \qquad (17)$$

Table 3 Sample convergence sequence

Iteration	f_w''	Γ_{qw}	$X_{N_{2w}}$	X_{CO_w}
Initial	0.50000	−2.5000	0.70000	0.15000
1	0.49712	−2.8344	0.66184	0.19428
2	0.51077	−3.1171	0.66215	0.20272
3	0.51224	−3.1584	0.66278	0.20284
4 and 5	0.51226	−3.1589	0.66278	0.20284

Conditions: $T_w = 4000$°R, $T_e = 12590$°R
$p_e = 5.85$ atm, $R_B = 1.01$ ft
$\eta_\infty = 5.0, \Delta\eta = 1/256$, slow reaction

Final errors: $(\epsilon, \epsilon_F, \epsilon_D) = 0.66 \times 10^{-6}$
$0.15 \times 10^{-9}, 0.65 \times 10^{-6}$

Table 4 Step size, nitric oxide, and precision checks

Case[a]	ν	$(\Delta\eta)^{-1}$	Cycles	Converged surface, $(\ )_w$, values						Errors	
				f_w''	X_{N_2}	$X_{O_2}(10^2)$	$X_{CO}(10^4)$	$-\Gamma_q$	$\dot{m}_S(10^2)$	ϵ_F	ϵ_D
1	7	256	4	0.46184	0.72176	0.58137	0.65009	3.2669	0.94386	0.387(−10)	0.115(−5)
2	7	256	4	0.46195	0.72176	0.58143	0.65006	3.2692	0.94389	0.244(−5)	0.252(−4)
3	6	256	4	0.45951	0.71974	0.59266	0.64944	3.2618	0.94993	0.792(−6)	0.246(−4)
4	6	128	4	0.45935	0.71973	0.59582	0.64937	3.2569	0.95001	0.875(−6)	0.167(−4)
5	6	64	4	0.45810	0.71960	0.59507	0.64840	3.2111	0.95121	0.299(−5)	0.367(−3)
6	6	32	4	0.45256	0.71921	0.60423	0.64415	3.0124	0.95607	0.142(−5)	0.189(−2)
7	6	16	5	0.44231	0.71964	0.61456	0.63749	2.6607	0.96149	0.187(−5)	0.979(−2)
8	6	8	63	0.43535	0.73556	0.66164	0.57767	2.3517	0.96545	0.929(−4)	0.697(−0)

[a] Notes: 1) Cases 1,2 (ν = 7) include NO; Cases 3–8 (ν = 6) exclude NO. 2) Case 1 double precision; Cases 2–8 single precision. 3) Cycles are number of iterations to achieve convergence. 4) All aforementioned cases based on: T_w = 3000°R, T_e = 12,590°R, p_e = 5.85 atm, R_B = 1.0 ft, slower kinetics 5) All previous cases initiated with starting guesses: f_w'' = 0.5, Γ_{qw} = −3.0, $X_{N_{2w}}$ = 0.70, X_{O_2N} = 0.006.

after taking note of Van't Hoff's isochore. This procedure when compared to exact values for CO and CO_2 (from JANAF[8]), e.g., led to average inaccuracies for the 900 ≤ T, °R ≤ 9900 range of 0.12, 0.01% in ΔF^0, 1.5, 0.05% in Δh^0, and 1.5, 0.6% in h^0, respectively, which were considered well within that required. The equilibrium constants $K_p = \exp(-\Delta F^0/RT)$ are correspondingly accurate. In contrast to the 3ν polynomial coefficients used here, an equivalently accurate description of the four properties of each species would entail evaluation and storage of $6(2\nu - k)$ coefficients, and moreover would violate the consistency implied by Eq. (17) as well as those for heat of reaction and specific heat statements.

Only binary diffusion coefficients were required in view of Eq. (15), and these as well as pure component viscosities and thermal conductivities are readily available.[9] The binary diffusion coefficients and mixture viscosities and conductivities are appreciably simplified on the basis of the Bartlett, Kendall, and Rindall[7] least-square fit constants (F_i) and an associated reference self diffusion coefficient. The $36\mathfrak{D}_{ij}$ approximated by

$$\mathfrak{D}_{ij} = (\mathfrak{D}_{ii})_{ref}/F_iF_j \tag{18}$$

for a 9 component O-N-C system results in an average error of 1.3% and a maximum error of 5.2% for all pairs. In contrast, were all $\mathfrak{D}_{ij}$ assumed equal the errors would be 24.2% and 63.4%, respectively. The F_i are shown in Table 2.

Similarly, the multicomponent viscosity $\mu = \mu(X_i,\mu_j,\mathfrak{D}_{ij})$ and conductivity κ are reducible to dependence upon X_j,F_j, $(\mathfrak{D}_{ii})_{ref}$, and collision integrals for the assumed (Leonard-Jones for molecule-molecule, hard sphere for atom-atom and atom-molecule) interaction potential model.[2,9] Effectively, all interaction potential details are absorbed into the F_i, and Wilke type mixture property approximations reduce the evaluations to single summations over X_j,F_j,m_j, etc. while preserving a realistic description of temperature, pressure, and composition effects. The system to be integrated after specification of the physical properties is equivalent to $(5 + k + \nu)$ first-order differential equations with initial values specified at the surface (η = 0). In principle a unique set of values, $y_i(0)$ say, lead to appropriate $y_i(\infty)$ in the asymptotic sense, i.e., $y_i'(\infty) = 0$. Some care was exercised to define acceptable errors in $y(\infty)$ and $y_i'(\infty)$. An over-all root-mean-square error was defined as

$$\epsilon = (\epsilon_F^2 + \epsilon_D^2)^{1/2} \tag{19}$$

in terms of function and derivative errors

$$\epsilon_i = \left\{\sum_{j=1}^{k+1} [\Delta y(\infty)]^2\right\}^{1/2} \qquad (i = F,D) \tag{20}$$

Here $\Delta y(\infty)$ represents the difference between integrated and required external edge conditions for the $(k + 1)$ parameters replaced by initial conditions specified at η = 0 (i.e., f_w'', Γ_{qw},X_{iw} with $(i = 1, \ldots, k - 1)$. $\epsilon \leq 10^{-4}$ was deemed satisfactory. When such criteria were not met the $(k + 1)$ initial values were modified by application of Newton-Raphson interation to determine correctors such that $\Delta y(\infty)$ is in principle driven to zero on the subsequent integration.

Table 3 illustrates a typical convergence sequence with the correctors being clear from the differences between successive initial conditions. Table 4 displays the results of an integration step size ($\Delta\eta$) check, the influence of omission or inclusion of NO as a component, and a single and double precision comparison. The convergence criterion here is ϵ_F within 10^{-4} with ϵ_D simply noted to indicate the closeness of asymptotic achievement in each instance. Cases 1 and 2 show a negligible NO effect. It is evident that $\Delta\eta \lesssim 0.01$ furnishes quite adequate accuracy for asymptotic solutions. Case 8 uses an extreme $\Delta\eta$ to show the excessive number of iterations necessary to converge and the rather large ϵ_D then remaining. Results included in the remaining part of this paper were based on $\Delta\eta$ = 1/256, ν = 6, single precision, correctors $\leq 10^{-4}$, and η_∞ = 5.

Table 5 Surface compositions for graphite oxidation, T_e = 12,590°R

Reaction	p_e, atm	R_B, ft	T_w, °R	X_{N_2}	X_{O_2}	X_{CO}	X_N	X_O	X_{CO_2}
Slow	5.85	1.0	2250	0.7476	0.1966	0.2670(−9)	0.1054(−16)	0.1309(−7)	0.5583(−1)
			3000	0.7177	0.9951(−3)	0.1619(−3)	0.1010(−11)	0.4155(−6)	0.2811
			4000	0.6628	0.3443(−5)	0.2028	0.5464(−8)	0.2394(−5)	0.1344
			5000	0.6170	0.1271(−6)	0.3802	0.9534(−6)	0.7260(−5)	0.2415(−2)
Fast			1500	0.7479	0.1948	0.3571(−14)	0.1134(−26)	0.6658(−13)	0.5721(−1)
			3000	0.6470	0.3302(−10)	0.2682	0.9490(−12)	0.7569(−10)	0.8480(−1)
Slower			3000	0.7025	0.2000(−1)	0.3334(−4)	0.1012(−11)	0.1863(−5)	0.2594
			5000	0.6614	0.1337(−2)	0.2037	0.9868(−6)	0.7447(−3)	0.1327
Fast		0.1	3000	0.6710	0.2458(−9)	0.1766	0.9767(−12)	0.2065(−9)	0.1523
		0.01		0.6935	0.1830(−8)	0.9136(−1)	0.9929(−12)	0.5635(−9)	0.2151
	0.585	1.0		0.6444	0.3537(−10)	0.3222	0.3026(−10)	0.2477(−9)	0.3335(−1)
	0.0585			0.6513	0.3452(−10)	0.3377	0.9622(−11)	0.7739(−9)	0.1092(−1)
	0.585	0.1		0.6590	0.2952(−9)	0.2625	0.3060(−11)	0.7157(−9)	0.7848(−1)

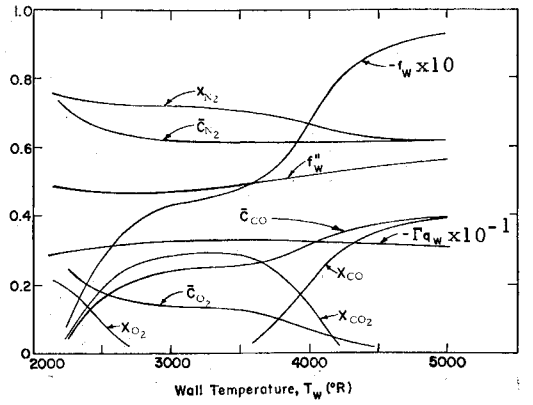

Fig. 1 Surface temperature concentrations and similarity flux parameters. Dependence on temperature for slow kinetics, R_B = 1.0 ft, p_e = 5.85 atm, T_e = 12,590°R.

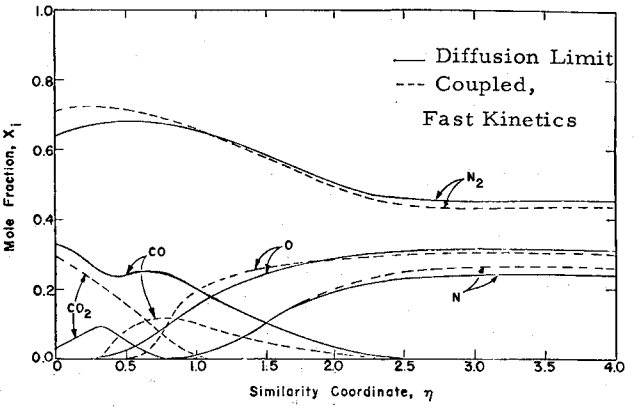

Fig. 2 Comparison of concentration profiles for diffusion limit and coupled models. Fast kinetics, R_B = 1.0 ft, p_e = 5.85 atm, T_e = 12,590°R, T_w = 2000°R. Diffusion limit.[3]

IV. Results and Discussion

A summary of converged surface values is included in Tables 5 and 6. The rapid depletion of oxygen with increasing surface temperature and its relative consumption for the several rate models are of special interest. It is fundamental to understanding both the large departures of the oxidation process from rate "control" and the numerical difficulties involved in achieving converged solutions. Table 5 indicates that orders of magnitude changes in X_{O_2}, X_O, X_{CO}, and X_{CO_2} at the surface occur with comparatively small T_w increments. Of course, all six components are not of equal importance for a given surface state. In particular, the oxide is more plentiful in CO_2 form at lesser temperatures and in the monoxide form at higher temperatures.

Table 6 shows corresponding surface flux parameters and the reduction of mass and heat transfer to equivalent 1 ft radius and 1 atm pressure levels by use of the similarity form $\dot{m}_w(R_B/p_e)^{1/2}$ etc. Separate calculations were conducted by the Aerotherm Corporation as part of the program.[2] The basis was an integral spline technique modified for the present purposes from a rather general Integral Matrix Program.[10] However, the numerical method and convergence procedures were substantially different. Together they supplied both further support to the solutions and an indication of differences resulting from distinct transport and thermodynamic property representations and computational methods. The agreement was considered quite good.

The graphical representation in Fig. 1 helps to clarify the behavior. Surface mole fractions X_{N_2}, X_{O_2}, X_{CO}, and X_{CO_2}, "element" mass fractions (from all sources) $\bar{c}_{N_2}$, $\bar{c}_{O_2}$, and $\bar{c}_{CO}$, and flux parameters Γ_{qw}, f_w'', and f_w' are shown for $2000 \leq T_w$, °R ≤ 5000. Of note are the rapid disappearance of oxygen, the relative insensitivity of Γ_{qw} and f_w'', the plateau forming tendency of f_w, and the dominance of CO and CO_2 in fairly distinct temperature ranges. Qualitatively, the same behavior is found with other rate specifications but with increasingly rapid kinetics implying a shift towards lesser temperatures for similar effects.

The element mass fractions ($\bar{c}_{i_w}$) exhibit relatively slow changes with T_w in contrast to the mole fraction which amount to orders of magnitude. This proves to be of some importance in selection of working parameters for which initial guesses are required. For numerical integration the $\bar{c}_i$ are preferable and in some cases virtually essential in practice.

Figure 2 compares entire boundary-layer profiles for the mole fractions (for the coupled fast reaction at T_w = 2000°R) with a previous[3] prediction which was based on a diffusion limit model. The important components are clearly O, CO, and CO_2. The fundamental origin of differences in mass transfer between diffusion limit and surface coupled models are apparent here. The relative magnitudes of CO and CO_2 concentrations adjacent to the surface are inverted for the two models, and in the coupled case CO is virtually absent at this surface temperature. Specific values are shown in Table 7. A second example of typical boundary-layer profiles for fast kinetics and T_w = 3000°R is provided in Fig. 3, including velocity, temperature, and the "element" mass fractions.

Mass flux from the surface as a consequence of the oxidation process is shown in Fig. 4 for all three rate descriptions, R_B = 1.0 ft, and p_e = 5.85 atm. A qualitative description includes an initial region of rapidly increasing surface mass flux followed by successive transitions to relative plateaus. Two plateaus are evident for the present graphite oxidation model and their magnitudes are relatively independent of the rate specifications.

Fundamentally, the appearance of plateaus is associated with the earlier mentioned abundance of first CO_2 and later

Table 6 Surface mass, momentum, and energy transfer results for graphite oxidation, T_e = 12,590°R

Reaction	p_e, atm	R_B, ft	T_w, °R	$-f_w$	f_w''	$-\Gamma_{qw}$	$\dot{m}_w \times 10^3$, lb/ft² sec	$\dot{m}_w(R_B/p_e)^{1/2} \times 10^{-3}$, lb/sec(ft³atm)$^{1/2}$	$-q_w(R_B/p_e)^{1/2}$, Btu/sec(ft³atm)$^{1/2}$
Slow	5.85	1.0	2250	0.00847	0.4796	3.038	1.941	0.8024	349.5
			3000	0.04336	0.4691	3.230	9.735	4.025	364.1
			4000	0.06735	0.5112	3.159	13.87	5.737	326.7
			5000	0.09234	0.5572	3.059	17.67	7.306	293.9
Fast			1500	0.00818	0.4358	2.705	2.015	0.8330	334.3
			3000	0.07149	0.4858	3.074	15.30	6.328	330.4
Slower			3000	0.04009	0.4730	3.224	8.976	3.711	362.3
			5000	0.06966	0.5391	3.165	13.79	5.702	314.6
Fast		0.1	3000	0.06134	0.4799	3.130	42.25	5.525	342.3
		0.01		0.05297	0.4748	3.179	116.0	4.798	352.9
	0.585	1.0		0.07226	0.4625	3.597	5.055	6.609	481.1
	0.0585			0.06979	0.4351	3.826	1.589	6.568	604.4
	0.585	0.1		0.06567	0.4582	3.620	14.70	6.078	489.9

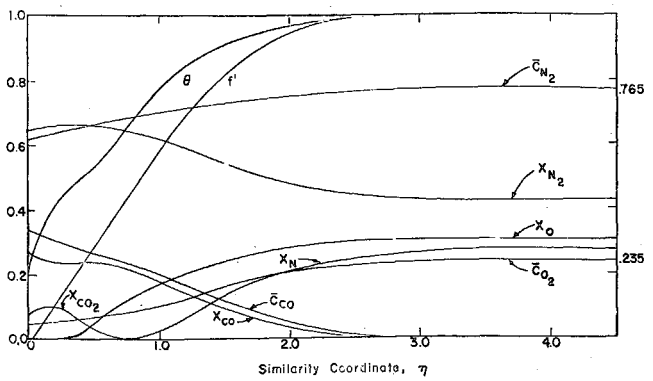

Fig. 3 Typical boundary-layer profiles: concentrations, temperature and velocity for fast kinetics, R_B = 1.0 ft, p_e = 5.85 atm, T_e = 12,590°R, T_w = 3000°R.

CO as the surface temperature is increased. The plateau regions are essentially temperature intervals within which the oxidation process is governed by the oxygen diffusion rate to the surface with all other component proportions remaining relatively fixed. From Fig. 1, for example, for slow kinetics it is evident that oxygen is dominant in uncombined form somewhat below 2500°R and rapidly vanishes thereafter. CO_2 dominance extends over the 2500–3800°R interval and CO then rapidly appears. Since nitrogen levels are relatively unaffected, such changes account for the overall fixed level consisting of all oxygen and carbon in the assumed gas phase model. The mass flux variation with T_w may then be described at "low" temperatures by a "reaction controlled limit" in which oxygen proves plentiful for some prescribed rate, and a series of "diffusion controlled limit plateaus" in which one component is dominant. Each such limit is joined to the next by a "transition region."

The essential point is that the number of diffusion limit plateaus is predetermined by the complexity of the gas model and the nature of the equilibrium (mass action) relations. Although multiple recession rate plateaus may be expected, the temperature interval for which such plateaus are actually present depends upon both the diffusive processes within the boundary layer and the speed of the reaction. The affect of the back reaction at the surface is to introduce a slight decrease in mass flux along the plateau with increasing temperature.

Energy transfer to the boundary is shown in Fig. 5. The lower plateau range involves 15% higher heat flux levels then the trend with surface temperature in the final diffusion limit range. Differences resulting from the flux integration and integral spline calculations are apparent here but are only of order a few percent. For reference, Fay and Riddell[11]

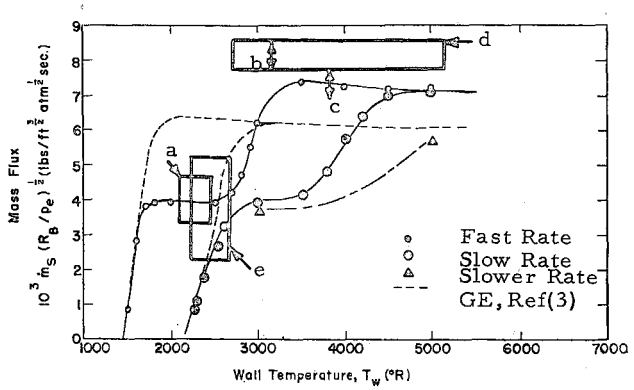

Fig. 4 Graphite oxidation rate dependence on surface temperature, R_B = 1.0 ft, p_e = 5.85 atm, T_e = 12,590°R. Experimental results are shown by *a*, *b*, and *c* (Ref. 12) and *d* and *e* (Ref. 13).

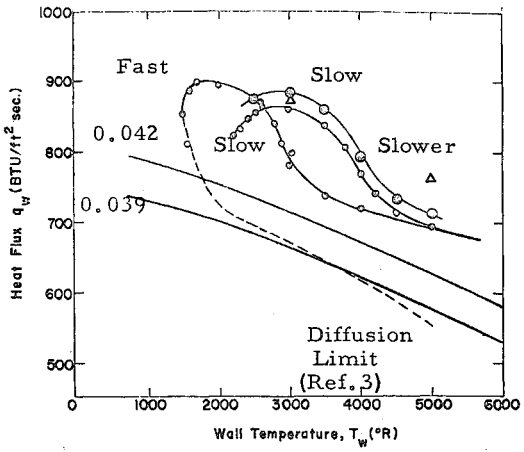

Fig. 5 Heat flux dependence on surface temperature, R_B = 1.0 ft, p_e = 5.85 atm, T_e = 12,590°R. Large circles and triangles refer to ManLabs calculations, small circles refers to Aerotherm calculations. Curves designated by 0.042 and 0.039 refer to ratios of $q_w(R_B/P_e)^{1/2}/(h_e - h_w)$ based on the Fay-Riddell relation.

forms and an uncoupled diffusion limit result[3] are also included.

Lastly, Fig. 6 presents a comparison of familiar similarity scaling according to $(p_e/R_B)^{1/2}$ with the results of Table 6. A surface temperature of 3000°R was chosen so as to examine the middle of the transition region for fast rate kinetics between the two-oxide plateaus (Fig. 4). As expected, in view of Eqs. (5) and (12), $q_w(R_B)$ and $\dot{m}_w(p_e)$ show reasonably good agreement with similarity scaling. Note from Table 1, however, that the reaction order was $\frac{1}{2}$. The alternate dependences, $\dot{m}_w(R_B)$ and $q_w(p_e)$ do show departures from the reference slopes, and some care should be exercised in general in transferring transition region predictions.

Present results may be compared with earlier graphite oxidation exact evaluations[3] in which diffusion control was assumed and plausible transitions suggested to connect to low temperature reaction control behavior. Those results are included in Figs. 2, 4, and 5.

The disagreement takes two forms and is most apparent from Fig. 4. The first relates to the magnitude of the ultimate (CO) diffusion controlled plateau which proves to be somewhat greater (17%) for the present work. More important in the limit model is the single plateau which fails

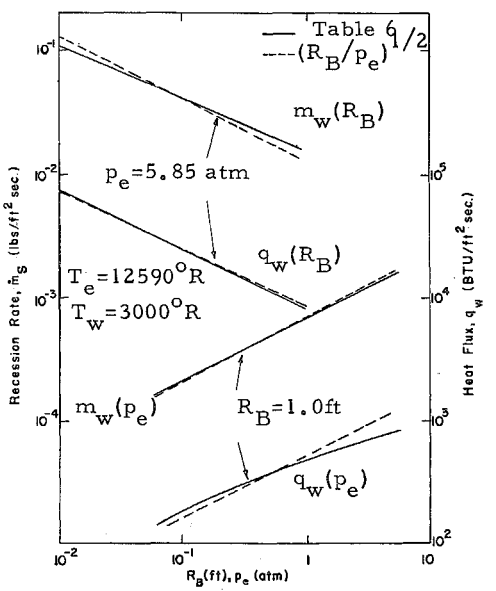

Fig. 6 Effects of body radius and pressure in transition region. Fast kinetics, T_w = 3000°R.

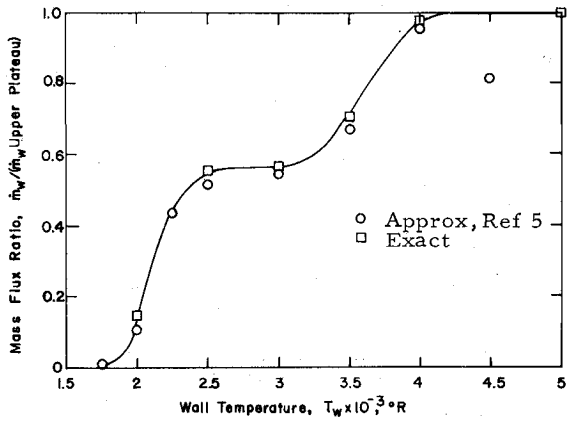

Fig. 7 Approximate and exact graphite oxidation rates. Slow kinetics, R_B = 1.0 ft, p_e = 5.85 atm, T_e = 12,590°R.

to distinguish between the wide difference in expected mass transfer magnitudes that occur in temperature ranges of practical interest. In essence, the equilibrium (diffusion limit) model corresponds to an assumption of extremely fast kinetics such that the lower (CO_2) plateau is naturally present at surface temperatures below 1000°R. The results for that lower plateau, although not shown in Fig. 4, are asymptotic to the same (i.e., 4.0) level[3] as the present finite rate solutions despite the discrepancy for the upper plateau.

Experimental bands[12,13] are also shown in Fig. 4 to illustrate the confusion that may arise when interpreting the validity of specific rate descriptions. Uncoupled solutions suggest that slow kinetics are valid. The coupled model makes evident that agreement with the two plateau results is preferable.

The appearance of multiple plateaus in the presence of several oxidation by products has been noted before by Welsh and Chung.[5] Their approximate analysis of graphite oxidation assumes simplified transport property descriptions such that λ and the Schmidt number are constant, neglects the pressure gradient contribution to the momentum balance, and treats oxygen as a single particle species. Some results for this model are displayed in Fig. 7 and Table 8, which are based on modified slow kinetics, i.e., $k_{O_2} = 5.36 \times 10^5$ lb/ft^2 sec atm$^{1/2}$), a Schmidt number of 0.72, $\lambda = 0.44$ and an external edge mass concentration for oxygen equal to 0.23. At T_w = 3000 and 4000°R, i.e., in the vicinities of the plateaus, the approximate model predicts 33–40% larger mass fluxes than an exact solution. Nevertheless, the normalized variations with each based upon its own upper plateau level indicates an excellent comparison (Fig. 7), especially on consideration of the relative simplicity of application of the Welsh and Chung model. The primary qualitative behavior is consistent with exact results while differences in transitions, magnitudes and extent of plateaus is undoubtedly related to the somewhat poorer oxygen descriptions as indicated by the surface mass fraction comparison in Table 8.

In summary the coupling of the surface reaction to the boundary-layer diffusion processes results in multiple plateaus as in an earlier approximate analysis but with appreciable numerical differences. The existence of such plateaus is predetermined by examination of the temperature dependence of the associated equilibrium constants. However, there is a strong dependence of the qualitative description on the magnitudes of the rate parameters such that the extent or existence of some plateaus may be in question. In the examples that have been cited the relative reaction speed results in the absence of a lower (CO_2) plateau in the presumed equilibrium (diffusion limit) case, a distinct pair of plateaus for so-called fast kinetics, and a smearing out of an actual upper (CO) plateau for a possible slower kinetics description.

Table 7 Model influence on surface concentrations (Fig. 2 conditions)

Component	Mole fraction, X_{iw}	
	Diffusion limit basis	Coupled (fast) basis
O_2	1.1×10^{-20}	6.9×10^{-6}
CO	0.32	8.4×10^{-8}
CO_2	4.4×10^{-2}	0.29

Appendix

The conservation equations and their boundary layer approximation are available in several sources and are not repeated here.[2,9,11] The similarity form makes use of the coordinates

$$\eta = \frac{(\rho u)_e r}{(2\xi)^{1/2}} \int_0^y \left(\frac{\rho}{\rho_e}\right) dy, \quad \xi = \int_0^x (\rho\mu')_w u_e r^2 dx$$

in place of (x,y), and a modified stream function $f(\eta) = \Psi/(2\xi)^{1/2}$ where the stream function itself satisfies $\Psi_y = \rho u r$ and $\Psi_x = -\rho v r$. Then $f' = u/u_e$ and for the surface mass flux

$$(\rho v)_w = -[2u_e(\rho\mu)_w/x]^{1/2} f(0)$$

The pressure gradient parameter, $\beta = 2d(\ln u_e)/d(\ln \xi)$, has been taken to be $\frac{1}{2}$ for a hemisphere in Eq. (1b).

The diffusion contribution to the mass flux is given by

$$J_{mi} = \sum_j (m_i m_j / m^2) \rho D_{ij} \partial X_j / \partial y$$

and its equivalent similarity form by

$$J_i = [c_p(2\xi)^{1/2}/\rho\kappa u_e r] J_{mi} = \sum_j (m_i m_j / m^2) L_{ij} \partial X_j / \partial \eta$$

A solid oxide correction factor,

$$a^{-1} = 1 - (m_{AO_y}/m_S) z_1$$

appears in Eq. (8) and again in Eq. (12) to relate the mass and energy conversion rate to that convected away. Similarly, an "over-all Δh for oxidation" factor appears in Eq. (12) as

$$H = (\Delta\bar{h})_S + [(1-a)/a]\bar{h}_{AO_y}(s) + (m_O/m_S) z_0 \bar{h}_{\text{oeff}}$$

to account for that portion of boundary-layer oxygen not included as parts of the g_{O_2} and g_O fluxes. The individual con-

Table 8 Approximate and exact solutions comparison for graphite oxidation modified slow reaction, R_B = 1.0 ft, p_e = 5.85 atm, T_e = 12590°R

T_w, °R	$\dot{m}_w$(lb/ft^2 sec)		$\dot{m}_w/\dot{m}_w$ (upper plateau)		Total mass fraction of surface oxygen	
	Approx.[5]	Exact	Approx.[5]	Exact	Approx.[5]	Exact
2000	0.257(−2)	0.266(−2)	0.101	0.144	1.85(−1)	1.95(−1)
2500	1.314(−2)	1.028(−2)	0.515	0.558	2.27(−3)	1.27(−3)
3000	1.39(−2)	1.043(−1)	0.545	0.566	1.53(−5)	7.95(−6)
3500	1.71(−2)	1.291(−2)	0.670	0.701	6.24(−7)	3.81(−7)
4000	2.43(−2)	1.793(−2)	0.955	0.975	7.90(−8)	1.91(−7)

tributions include an $h_{O_{eff}}$ term which is the h_{OgO} contribution for oxygen participating in the surface reaction; the remaining two terms together imply the gaseous heat of reaction seen by the layer when a solid deposit is involved.

References

[1] Kaufman, L. and Nesor, H., "Stability Characterization of Refractory Materials Under High Velocity Atmospheric Flight Conditions," AFML-TR-69-84, Pt. I, Vol. I, March 1970, ManLabs Inc., Cambridge, Mass.

[2] Bernstein, H. and Baron, J. R., "Stability Characterization of Refractory Materials Under High Velocity Atmospheric Flight Conditions," AFML-TR-69-84, Pt. IV, Vol. II, Dec. 1969, ManLabs Inc., Cambridge, Mass.

[3] Scala, S. M., "The Ablation of Graphite in Dissociated Air," Paper 62-154, 1962, IAS.

[4] Gilbert, L. M., "The Hypersonic Diffusion Controlled Oxidation of Tungsten," Rept. R67SD38, 1967, General Electric Co., King of Prussia, Pa.

[5] Welsh, W. E. and Chung, P. M., "A Modified Theory for the Effect of Surface Temperature on the Combustion Rate of Carbon Surfaces in Air," *Proceedings of the Heat Transfer and Fluid Mechanics Institute*, Stanford University Press, 1963, pp. 146–159.

[6] Nachtsheim, P. R., "Multicomponent Diffusion on Chemically Reacting Laminar Boundary Layers," *Proceedings of the Heat Transfer and Fluid Mechanics Institute*, Stanford University Press, 1967, pp. 58–87.

[7] Bartlett, E. P., Kendall, R. M., and Rindal, R. A., "Unified Approximation for Mixture Transport Properties for Multicomponent Boundary Layer Applications," Rept. 66-7, Pt. IV, March 1967, Aerotherm Corp., Palo Alto, Calif.

[8] JANAF Thermochemical Data, Dow Chemical Co., Midland, Mich., 1960.

[9] Hirchfelder, J. O., Curtiss, C. F., and Bird, R. B., *Molecular Theory of Gases and Liquids*, Wiley, New York, 1966.

[10] Kendall, R. M. and Bartlett, E. P., "Nonsimilar Solution of the Multicomponent Laminar Boundary Layer by an Integral Matrix Method," Rept. 66-7, Pt. III, March 1967, Aerotherm Corp., Palo Alto, Calif.

[11] Fay, J. A. and Riddell, F. R., "Theory of Stagnation Point Heat Transfer in Dissociated Air," *Journal of the Aeronautical Sciences*, Vol. 25, No. 2, Feb. 1958, pp. 73–85.

[12] Diaconis, N. S., Gorsuch, P. D., and Sheridan, R. A., "The Ablation of Graphite in Dissociated Air, Part 2, Experiment," Paper 62-155, 1962, IAS.

[13] Metzger, J. W., Engel, M. J., and Diaconis, N. S., "Oxidation and Sublimation of Graphite in Simulated Re-Entry Environments," *AIAA Journal*, Vol. 5, No. 3, March 1967, pp. 451–460.

AUGUST 1971 AIAA JOURNAL VOL. 9, NO. 8

Behavior of a Liquid Jet near the Thermodynamic Critical Region

J. A. NEWMAN* AND T. A. BRZUSTOWSKI†
University of Waterloo, Waterloo, Ontario, Canada

As thrust levels in modern rocket engines have risen, combustion chamber pressures in excess of the fuel and oxidizer critical pressures can be expected. This study concerns itself with how these particular conditions affect the atomization and mixing processes accompanying the injection of liquid propellants into a gaseous environment. The paper describes an experimental analysis in which a liquid issues into a gas whose pressure and temperature are close to (and often exceed) the liquid critical pressure and temperature. The data include observations of the geometric, dynamic, and thermal characteristics of the spray. A theoretical analysis is performed in which the two-phase spray is treated as a turbulent submerged jet. Verified mechanisms of turbulent mixing are used where possible. The equations for the constancy of mass, momentum, and energy and a modified jet propagation equation are solved numerically to yield information about the axial velocity, concentration, and temperature difference decay rates.

Nomenclature

a = liquid to environmental gas-density ratio ρ_l/ρ_s
A = area
$b_i,\bar{b}_i$ = boundary-layer thickness, b_i/r_o
$b_M,\bar{b}_M$ = main region jet radius, b_M/r_o
C = liquid to gas mass-flow-rate ratio $\dot{m}_l/\dot{m}_g$
C_l = liquid mass fraction in liquid gas mixture $\dot{m}_l/(\dot{m}_l + \dot{m}_g)$
c_p = specific heat at constant pressure
f,g,h = velocity, concentration, and temperature distribution functions
H = heat-transfer coefficient
K = $[1 - \Delta\bar{T}_m g_M(1 - S)]$
k = thermal conductivity
$\dot{m}$ = mass flow rate
Q = liquid-to-gas heat capacity ratio
P,P_r = pressure, P/Pc
$R,\bar{R}$ = jet radius (equals r_2 in initial region, b_M in main region), R/r_o
$\mathcal{R}$ = gas constant
$r,\bar{r}$ = radial coordinate, r/r_o
r_o = injector radius
$r_1,\bar{r}_1$ = location of inner boundary in initial region, r_1/r_o
$r_2,\bar{r}_2$ = location of outer boundary in initial region, r_2/r_o
r_d = droplet radius
S = liquid to environmental temperature ratio T_{lo}/T_s
t = time
T = temperature
$\Delta\bar{T}$ = $(T_s - T)/(T_s - T_{lo})$
U = axial velocity
$\bar{U}$ = U/U_o
$x,\bar{x}$ = axial coordinate, x/r_o
α = thermal diffusivity
ρ = density
σ = surface tension
μ = viscosity

Presented as Paper 70-8 at the AIAA 8th Aerospace Sciences Meeting, New York, January 19–21, 1970; submitted February 26, 1970; revision received March 4, 1971.

* Lecturer; presently Assistant Professor, Department of Mechanical Engineering, University of Ottawa. Member AIAA.

† Chairman, Department of Mechanical Engineering. Member AIAA.